

AdaptPrompt: Parameter-Efficient Adaptation of VLMs for Generalizable Deepfake Detection

YICHEN JIANG, University of Waterloo, Canada

MOHAMMED TALHA ALAM^{*†}, MBZUAI, UAE

SOHAIL AHMED KHAN, University of Bergen, Norway

DUC-TIEN DANG-NGUYEN, University of Bergen, Norway

FAKHRI KARRY, University of Waterloo, Canada

Recent advances in image generation have led to the widespread availability of highly realistic synthetic media, increasing the difficulty of reliable deepfake detection. A key challenge is generalization, as detectors trained on a narrow class of generators often fail when confronted with unseen models. In this work, we address the pressing need for generalizable detection by leveraging large vision-language models, specifically CLIP, to identify synthetic content across diverse generative techniques. First, we introduce Diff-Gen, a large-scale benchmark dataset comprising 100k diffusion-generated fakes that capture broad spectral artifacts unlike traditional GAN datasets. Models trained on Diff-Gen demonstrate stronger cross-domain generalization, particularly on previously unseen image generators. Second, we propose AdaptPrompt, a parameter-efficient transfer learning framework that jointly learns task-specific textual prompts and visual adapters while keeping the CLIP backbone frozen. We further show via layer ablation that pruning the final transformer block of the vision encoder enhances the retention of high-frequency generative artifacts, significantly boosting detection accuracy. Our evaluation spans 25 challenging test sets, covering synthetic content generated by GANs, diffusion models, and commercial tools, establishing a new state-of-the-art in both standard and cross-domain scenarios. We further demonstrate the framework's versatility through few-shot generalization (using as few as 320 images) and source attribution, enabling the precise identification of generator architectures in closed-set settings.

ACM Reference Format:

Yichen Jiang, Mohammed Talha Alam, Sohail Ahmed Khan, Duc-Tien Dang-Nguyen, and Fakhri Karray. 2025. AdaptPrompt: Parameter-Efficient Adaptation of VLMs for Generalizable Deepfake Detection. 1, 1 (December 2025), 21 pages.

1 Introduction

Deepfake technology has revolutionized modern media, but this advancement poses significant security risks, ranging from misinformation campaigns to privacy violations [5, 18, 48, 49]. As synthesis techniques evolve from Generative Adversarial Networks (GANs) [24] to Diffusion Models (e.g., Stable Diffusion, Midjourney) [46], a critical "generalization gap" has emerged. Traditional detectors, trained primarily on GAN-generated imagery, struggle to generalize to

^{*}Equal Contribution

[†]Corresponding author

Authors' Contact Information: Yichen Jiang, y92jiang@uwaterloo.ca, University of Waterloo, Canada; Mohammed Talha Alam, mohammed.alam@mbzuai.ac.ae, MBZUAI, UAE; Sohail Ahmed Khan, sohail.khan@uib.no, University of Bergen, Norway; Duc-Tien Dang-Nguyen, ductien.dangnguyen@uib.no, University of Bergen, Norway; Fakhri Karray, karray@uwaterloo.ca, University of Waterloo, Canada.

Permission to make digital or hard copies of all or part of this work for personal or classroom use is granted without fee provided that copies are not made or distributed for profit or commercial advantage and that copies bear this notice and the full citation on the first page. Copyrights for components of this work owned by others than the author(s) must be honored. Abstracting with credit is permitted. To copy otherwise, or republish, to post on servers or to redistribute to lists, requires prior specific permission and/or a fee. Request permissions from permissions@acm.org.

© 2025 Copyright held by the owner/author(s). Publication rights licensed to ACM.

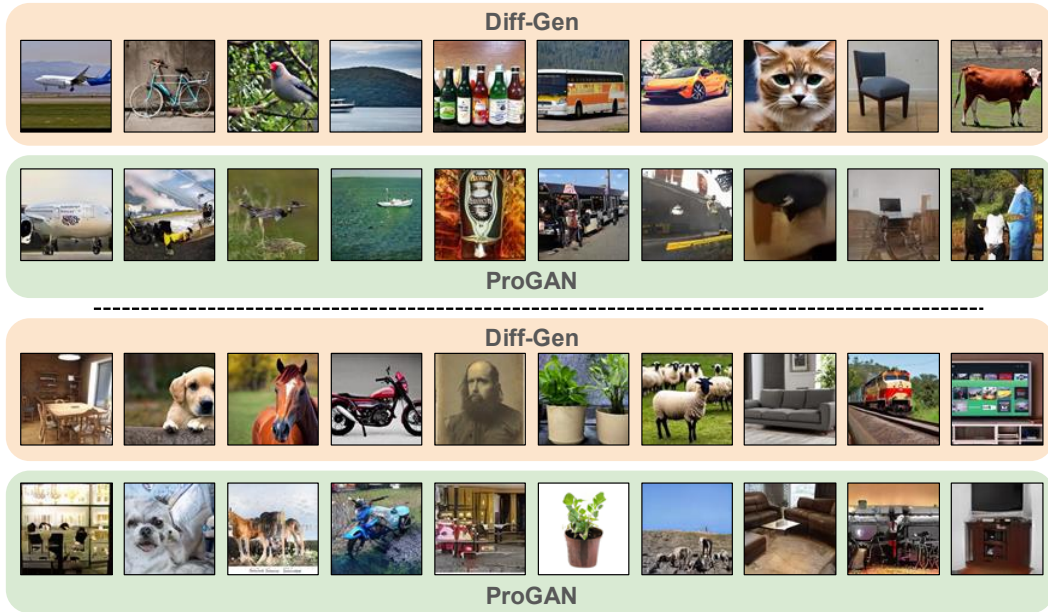


Fig. 1. Comparative visualization of the training datasets. The top row displays random samples from our proposed Diff-Gen dataset, generated via diffusion models, while the bottom row shows samples from the GAN-based ProGAN dataset. Both datasets share an identical class distribution covering 20 object categories (e.g., airplane, bird, bottle) to ensure fair comparison. Visually, Diff-Gen introduces distinct high-frequency noise artifacts compared to the structural periodic artifacts typical of ProGAN, challenging the detector to generalize beyond GAN-specific fingerprints.

diffusion-based synthetic media [1, 4, 11, 54]. This failure stems from the "sink label" problem: binary classifiers often learn specific GAN fingerprints (e.g., checkerboard artifacts) as the definition of "fake," consequently misclassifying unseen diffusion artifacts as "real" [39].

To address this, researchers have turned to Vision-Language Models (VLMs) like CLIP, leveraging their robust pre-trained feature spaces. While recent works have explored adapting VLMs via linear probing or fine-tuning [35, 39], these methods either fail to fully unlock the model's potential or suffer from overfitting. We hypothesize that a synergistic approach that combines visual adaptation to capture pixel-level artifacts and textual prompt tuning to align semantic anomalies can yield a more robust detector. Furthermore, the choice of training data is pivotal. Existing detectors trained on GAN-generated images fail to capture the high-frequency noise residuals characteristic of diffusion models. This raises a critical question: can a detector trained on diffusion-based noise patterns generalize backward to GANs and forward to commercial image generation tools more effectively than traditional approaches?

To answer this, we introduce Diff-Gen, a large-scale dataset comprising 100k diffusion-generated images that mirror the class distribution of the LSUN [53] real dataset, shown in Fig. 1. Unlike GANs, which leave distinct periodic fingerprints, diffusion models exhibit noise-like artifacts that existing datasets fail to capture. We further propose AdaptPrompt, a parameter-efficient transfer learning framework that optimizes both the visual and textual pathways of CLIP while keeping the backbone frozen. We conduct a comprehensive empirical analysis across 25 diverse test datasets, covering GANs, diffusion models, and commercial generators. Our contributions are summarized as follows:

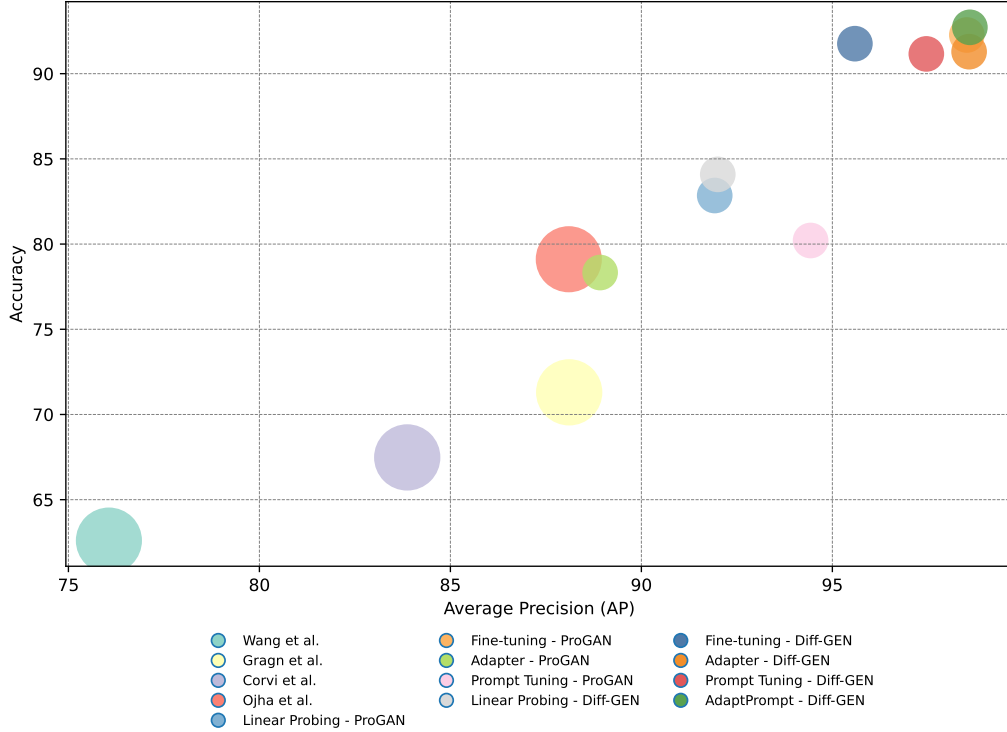


Fig. 2. Performance landscape of state-of-the-art deepfake detectors. This bubble chart plots Average Precision (AP) against Accuracy on the combined test set. The size of each bubble corresponds to the relative size of the training dataset used. Our proposed method, AdaptPrompt trained on Diff-Gen (green bubble), achieves the optimal trade-off in the top-right corner, demonstrating superior efficiency and performance compared to fully fine-tuned models and other parameter-efficient baselines.

- We introduce Diff-Gen, a novel training benchmark that captures the broad spectral characteristics of diffusion noise. We demonstrate that models trained on Diff-Gen exhibit significantly stronger cross-domain generalization compared to those trained on ProGAN [30].
- We propose AdaptPrompt, a unified transfer learning strategy that combines adapter networks and prompt tuning. We show via ablation that pruning the final transformer block of the vision encoder enhances the retention of high-frequency generative artifacts, boosting detection accuracy.
- We provide a comprehensive evaluation on 25 unseen datasets, establishing a new state-of-the-art for generalizable deepfake detection. In addition, we extend our framework to the task of source attribution, demonstrating high accuracy in identifying specific generator architectures.

This paper is organized as follows. Section 2 reviews related work in generative forensics and VLM adaptation. Section 3 details the AdaptPrompt methodology and the Diff-Gen dataset. Section 4 presents extensive experimental results, including spectral analysis and robustness checks. Finally, Section 5 concludes the study.

2 Related Work

2.1 Evolution of Generative Forensics

The rapid evolution of generative models has necessitated a parallel evolution in forensic detection. Early synthetic media generation relied on modifying existing images, such as facial manipulation or Photoshop editing [7, 43, 51]. With the advent of Generative Adversarial Networks (GANs) [24], research shifted toward identifying model-specific fingerprints [6]. Studies have demonstrated that GAN-generated images exhibit distinct spectral artifacts, often visible as periodic patterns in the frequency domain due to upsampling operations [2, 3, 15, 16, 22]. Consequently, many detectors focused on these visible traces [19, 20, 36] or manipulated facial regions [47].

However, the emergence of Diffusion Models [50] has complicated this landscape. Unlike GANs, diffusion models generate images via iterative denoising, resulting in fingerprints that resemble high-frequency Gaussian noise rather than structural periodicity. This shift renders frequency-based detectors less effective on modern deepfakes (e.g., Stable Diffusion [46], DALL-E [41]), highlighting the need for more agnostic detection features.

2.2 The Generalization Dilemma

A critical challenge in deepfake detection is the "generalization dilemma" [11, 34, 56], where classifiers perform well on seen generator architectures but fail on unseen ones. Wang et al. [52] pioneered the study of cross-generator generalization, training a ResNet-50 [27] classifier on a large-scale dataset of 720,000 images, comprising 360,000 ProGAN fakes [30] and 360,000 LSUN real images [53]. While this approach generalized effectively to other GAN variants, subsequent work by Gragnaniello et al. [25] and Corvi et al. [13] revealed that such models struggle significantly when tested on diffusion-generated content.

This failure is largely attributed to the "sink label" problem identified by Ojha et al. [39]. Traditional binary classifiers tend to learn specific artifacts (e.g., GAN checkerboard patterns) as the definition of "fake." Consequently, when encountering diffusion-generated images that lack these specific artifacts, the model defaults to classifying them as "real" (the sink label). This insight suggests that instead of learning a decision boundary based on specific artifacts, detectors must leverage richer, more generalized feature spaces.

2.3 Adaptation of Vision-Language Models

To overcome the limitations of supervised training on limited forensic datasets, recent research has pivoted to leveraging pre-trained Vision-Language Models (VLMs) like CLIP [26, 29, 45]. VLMs offer a robust, semantically rich feature space learned from vast web-scale data. Ojha et al. [39] demonstrated that a simple linear classifier trained on frozen CLIP-ViT features achieves state-of-the-art generalization across both GANs and diffusion models, effectively mitigating the sink label problem.

Building on this, Khan and Dang-Nguyen [35] performed a systematic evaluation of transfer learning strategies for forensics, comparing Linear Probing, End-to-End Fine-tuning, and Parameter-Efficient Fine-Tuning (PEFT) methods [28]. Their findings indicate that lightweight adaptation techniques, specifically Adapter Networks [23] and Prompt Tuning [54], yield superior generalization compared to full fine-tuning, which is prone to overfitting. In this work, we extend these findings by proposing *AdaptPrompt*, a unified framework that synergizes visual adapters and textual prompt tuning to capture both pixel-level artifacts and semantic anomalies.

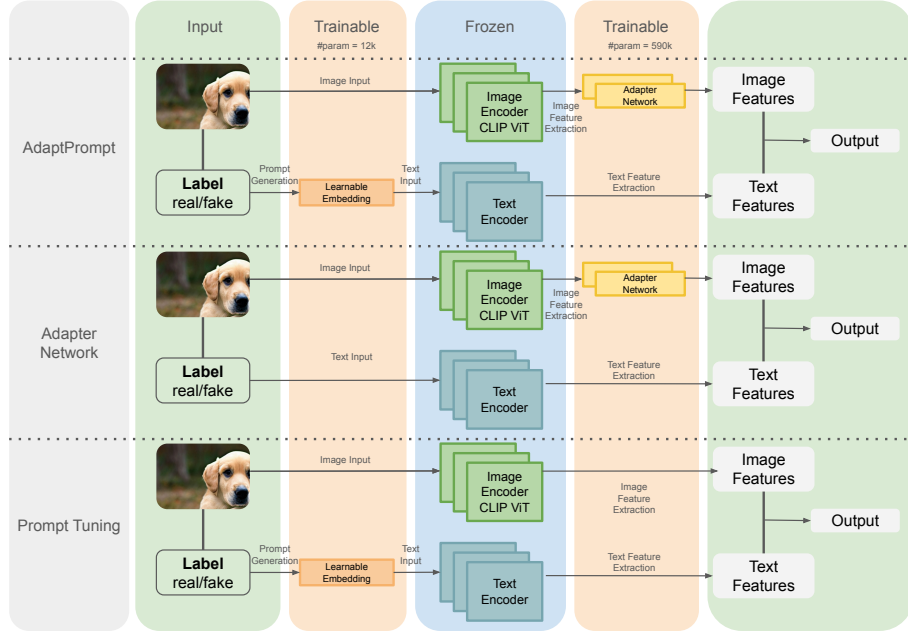


Fig. 3. **Architectural overview of the evaluated transfer learning strategies.** The diagram contrasts (top) our proposed AdaptPrompt, (middle) Adapter Network, and (bottom) Prompt Tuning. Blue blocks represent the frozen CLIP backbone (Image and Text Encoders), while orange/yellow blocks indicate trainable parameters. AdaptPrompt uniquely optimizes both modalities simultaneously: it injects a lightweight Adapter Network into the visual stream to capture pixel-level artifacts and utilizes Learnable Embeddings in the textual stream to align the semantic space, keeping the vast majority of CLIP parameters frozen to prevent overfitting.

3 Methodology

3.1 Problem Formulation

The objective of generalizable deepfake detection is to learn a binary classification function $f : \mathcal{X} \rightarrow \{0, 1\}$ that maps an input image $x \in \mathcal{X}$ to a label y , where $y = 1$ denotes a fake image and $y = 0$ denotes a real image. The critical challenge lies in the domain gap: models trained on a specific source distribution \mathcal{D}_S (e.g., GANs) must generalize to an unseen target distribution \mathcal{D}_T (e.g., Diffusion Models) where the generative artifacts differ significantly in spectral and spatial characteristics.

3.2 Preliminaries: CLIP-based Forensics

Our framework leverages Contrastive Language-Image Pre-training (CLIP) [45], which consists of a visual encoder \mathcal{V} and a text encoder \mathcal{T} . These encoders project images and text into a shared d -dimensional embedding space. Previous forensic approaches [35, 39] typically freeze the visual encoder \mathcal{V} and train a lightweight classifier (e.g., Linear Probing) on the extracted embeddings $z_v = \mathcal{V}(x)$. While effective, this approach treats the semantic features of CLIP as static, potentially discarding subtle high-frequency artifacts required for detection.

3.3 Proposed Framework: AdaptPrompt

To address the limitations of static feature extraction, we propose **AdaptPrompt**, a dual-modality transfer learning framework. As illustrated in Fig. 3, **AdaptPrompt** introduces two parameter-efficient components—a Visual Adapter and Learnable Text Prompts—while keeping the massive pre-trained backbone frozen to prevent overfitting.

3.3.1 Visual Adapter Network. Standard CLIP features are optimized for semantic alignment, making them invariant to the low-level noise residuals often present in deepfakes. To recover these artifact-centric features, we inject a lightweight Adapter Network [23] into the visual stream. Let $X \in \mathbb{R}^{B \times d_v}$ denote the image features extracted from the frozen encoder, where B is the batch size. The adapter functions as a residual bottleneck, formulated as:

$$Y = X + \alpha \cdot \text{MLP}(X) \quad (1)$$

where α is a scaling factor. The MLP consists of a down-projection $W_{down} \in \mathbb{R}^{d_v \times d_{mid}}$, a non-linear activation $\sigma(\cdot)$, and an up-projection $W_{up} \in \mathbb{R}^{d_{mid} \times d_v}$, such that:

$$\text{MLP}(X) = \sigma(XW_{down})W_{up} \quad (2)$$

By setting $d_{mid} \ll d_v$, the adapter acts as a bottleneck, forcing the model to learn a compact representation of generative fingerprints distinct from the semantic content.

3.3.2 Architectural Pruning Insight (The "v2" Variant). A key contribution of our work is the analysis of CLIP's layer-wise feature utility. We hypothesize that the final transformer blocks of CLIP are highly specialized for semantic abstraction, effectively "smoothing out" the pixel-level anomalies required for forensics. To test this, we truncate the visual encoder by removing the final transformer block and the projection head. In this configuration, denoted as **AdaptPrompt_v2**, the adapter receives features from the penultimate layer. These "rawer" structural features retain higher spectral energy in high-frequency bands, enabling the adapter to better distinguish diffusion noise from natural image statistics.

3.3.3 Textual Prompt Tuning. To complement the visual adapter, we employ Prompt Tuning [54] to learn task-specific text representations. Instead of relying on hand-crafted static prompts (e.g., "a photo of a fake"), which may be suboptimal, we optimize a sequence of continuous context vectors. The prompt P_c for class $c \in \{\text{Real}, \text{Fake}\}$ is constructed as:

$$P_c = [v_1, v_2, \dots, v_M, \text{CLASS}_c] \quad (3)$$

where $\{v_m\}_{m=1}^M$ are learnable context vectors (where $v_m \in \mathbb{R}^d$) and CLASS_c is the fixed embedding for the class name. These prompts are fed into the frozen text encoder \mathcal{T} to generate class embeddings $E_c = \mathcal{T}(P_c)$. This allows the model to learn a semantic definition of "fakeness" that aligns with the adapted visual features.

3.4 Optimization Objective

The model is trained end-to-end using a standard cross-entropy loss. The probability of an image x belonging to class c is computed via cosine similarity between the adapted visual features Y and text embeddings E_c :

$$p(y = c|x) = \frac{\exp(\langle Y, E_c \rangle / \tau)}{\sum_{j \in \{\text{Real}, \text{Fake}\}} \exp(\langle Y, E_j \rangle / \tau)} \quad (4)$$

where τ is a learnable temperature parameter. By updating only the adapter weights and prompt vectors, **AdaptPrompt** optimizes approximately 0.1% of the total parameters, ensuring high training efficiency.

Table 1. Generalization performance (Average Precision - AP). Comparison of detection AP scores on unseen test datasets. "Ours" refers to models trained on Diff-Gen. AdaptPrompt_v2 (bold) achieves state-of-the-art results, particularly on the challenging "Commercial Tools" and "Diffusion" subsets, outperforming the full Fine-Tuning baseline while using significantly fewer trainable parameters.

Method	Variant	Generative Adversarial Networks										Denoising Diffusion Models					FF++		mAP	
		Pro GAN	Big GAN	Cycle GAN	EG3D	Gau GAN	Star GAN	Style GAN	Style GAN-2	Style GAN-3	Taming-T	DALL-E(mini)	Glide	Guided	LDM	SD	SDXL	Deep Fakes	Face Swap	
Wang et al. (CVPR'20)	Blur+JPEG (0.1)	100.00	83.04	90.09	95.58	88.94	97.18	99.27	96.43	98.63	73.9	67.47	81.02	83.10	68.61	64.33	72.27	75.88	50.78	81.18
	Blur+JPEG (0.5)	100.00	82.63	94.71	55.32	96.62	93.88	93.25	88.64	85.33	59.78	60.92	69.75	65.11	60.24	52.14	65.92	64.33	49.76	72.65
Grage et al. (ICME'21)	ResNet-50 No Downsample	100.00	97.57	97.63	99.95	88.36	99.99	100.00	99.98	100.00	95.31	91.32	94.08	93.81	92.33	91.75	90.93	95.90	61.54	94.24
	ProGAN/LSUN Latent/LSUN	100.00	99.66	97.94	99.92	99.74	99.95	100.00	99.96	99.93	94.34	95.45	89.51	79.30	88.26	87.01	74.90	95.52	56.58	91.52
Ojha et al. (CVPR'23)	CLIP Linear Probing	99.99	98.73	98.92	79.58	99.74	96.06	95.73	95.81	92.21	97.12	96.84	93.85	92.09	95.71	93.58	88.55	77.48	75.87	93.05
	Linear Probing	99.94	97.77	98.53	99.48	99.69	99.80	95.53	94.88	99.54	97.74	95.65	97.25	92.14	95.94	92.24	94.09	80.07	76.58	95.22
Khan et al. (ICMR'24)	Fine Tuning	100.00	98.65	99.00	99.97	98.12	100.00	99.61	99.48	100.00	98.38	98.15	96.23	97.40	98.79	97.53	99.52	87.42	60.22	96.29
	Adapter	100.00	99.58	99.07	99.50	99.08	99.98	99.44	98.80	99.83	99.27	98.60	99.26	96.16	97.76	91.90	92.32	91.37	82.11	97.27
Ours_v0	Prompt Tuning	100.00	99.42	99.92	99.51	99.95	99.97	99.52	98.62	99.68	99.54	98.89	99.32	97.41	97.91	96.23	96.42	92.59	88.01	98.06
	Linear Probing_v0	97.64	74.51	71.70	98.00	71.56	80.04	99.18	95.14	99.72	99.22	97.98	83.45	96.19	92.97	99.89	99.53	47.65	55.70	87.50
Ours_v1	Fine Tuning_v0	99.90	70.93	60.61	100.00	61.54	99.72	98.76	88.79	100.00	99.62	99.31	92.89	97.93	99.86	99.97	99.95	63.09	55.57	91.73
	Adapter_v0	99.89	94.87	91.51	100.00	95.41	99.10	99.20	97.51	99.95	99.43	97.01	97.40	98.01	99.86	99.80	66.17	66.39	95.53	
Ours_v2	Prompt Tuning_v0	99.79	88.53	79.81	99.97	85.35	98.46	99.29	97.08	99.81	99.32	99.37	95.22	96.50	97.26	99.86	99.71	61.07	61.30	93.62
	AdaptPrompt_v0	99.87	91.53	89.59	99.95	89.69	98.69	98.91	96.84	99.72	99.09	99.08	95.15	96.04	97.71	99.98	99.73	63.95	65.01	94.50
Ours_v1	Fine Tuning_v1	99.41	65.50	52.75	100.00	65.88	99.48	97.93	97.96	100.00	99.52	99.16	93.43	97.23	99.71	100.00	99.98	54.37	52.73	90.44
	Adapter_v1	99.90	94.86	91.50	99.97	95.41	99.09	99.20	97.51	99.95	99.54	99.44	97.01	97.39	98.01	99.96	99.80	66.16	66.37	95.53
Ours_v2	Prompt Tuning_v1	99.79	88.53	79.81	99.97	85.35	98.46	99.29	97.08	99.81	99.32	99.37	95.22	96.59	97.26	99.86	99.71	61.07	61.30	93.62
	AdaptPrompt_v1	99.87	91.53	89.59	99.95	89.69	98.69	98.91	96.84	99.72	99.09	99.08	95.15	96.04	97.71	99.98	99.73	63.95	65.01	94.46
Ours_v2	Linear Probing_v2	98.53	83.86	75.70	96.59	79.07	95.88	98.99	95.01	99.56	99.25	99.81	85.50	95.98	92.76	99.85	99.78	63.09	55.57	89.81
	Fine Tuning_v2	99.77	70.84	59.23	100.00	62.49	99.02	97.87	98.50	100.00	99.56	99.55	97.55	97.35	99.75	99.99	99.94	62.06	53.54	91.43
Ours_v2	Adapter_v2	99.76	95.64	95.93	99.99	97.00	99.76	98.89	96.26	99.89	99.50	99.23	96.70	97.52	97.74	99.99	99.91	69.66	69.35	96.02
	Prompt Tuning_v2	99.78	90.29	89.93	99.85	90.70	99.80	99.17	95.91	99.85	98.77	98.47	95.10	95.56	96.72	99.74	99.52	55.98	60.52	93.88
Ours_v2	AdaptPrompt_v2	99.82	94.24	95.46	99.99	95.50	99.78	99.01	96.41	99.95	99.68	99.33	97.66	98.24	97.95	99.98	99.90	67.06	68.17	95.91

4 Experiments

4.1 Experimental Setup

4.1.1 Training Datasets. To investigate the impact of training data on generalization, we utilize two distinct datasets following the protocol established by Khan and Dang-Nguyen [35].

- **ProGAN:** A widely used GAN-based training set containing 720k images (balanced real/fake), where fakes are generated by ProGAN [30].
- **Diff-Gen (Ours):** Our dataset comprises of 100k diffusion-generated fakes and 100k real images sourced from LSUN [53]. The fake images are generated using state-of-the-art diffusion models to capture non-periodic noise artifacts. The text prompts follow the template '*A photo of a [class name]*', covering 20 distinct object categories to match the semantic distribution of the LSUN real subset. A Classifier-Free Guidance (CFG) scale of 7.5 was utilized to balance image fidelity and diversity.

4.1.2 Evaluation Benchmark. We evaluate our models on a comprehensive benchmark spanning 25 datasets, categorized into three families:

- (1) **GANs:** Includes ProGAN, StyleGAN variants, and BigGAN.
- (2) **Diffusion Models:** Includes Glide [38], LDM [46], and Stable Diffusion. For Glide and LDM, we average performance across three different configuration settings per model.
- (3) **Commercial Tools:** Includes high-fidelity images from Midjourney, DALL-E 3, and Adobe Firefly.

This diverse suite ensures that models are tested against architectures seen during training as well as completely unseen generative mechanisms. Detailed specifications for all 25 datasets are provided in Appendix A (Table 6).

Table 2. Generalization performance (Accuracy). Detailed classification accuracy scores corresponding to Table 2. Consistent with AP trends, AdaptPrompt_v2 demonstrates the highest average accuracy (92.72%), validating the hypothesis that simplifying the CLIP backbone (removing the last block) aids in retaining artifact-centric features.

Method	Variant	Generative Adversarial Networks										DALL-E(mini)	Denoising Diffusion Models					FF++		Avg. Acc
		Pro GAN	Big GAN	Cycle GAN	EG3D	Gen GAN	Star GAN	Style GAN	Style GAN-2	Style GAN-3	Taming-T		Glide	Guided	LDM	SD	SDXL	Deep Fakes	Face Swap	
Wang et al. (CVPR'20)	Blur+JPEG (0.1)	99.90	67.65	79.50	72.65	76.63	89.72	82.10	77.05	80.68	56.45	55.05	61.15	62.90	54.03	52.50	53.40	52.67	49.68	66.09
	Blur+JPEG (0.5)	99.65	58.13	77.80	50.30	79.99	69.80	62.30	53.42	51.05	51.90	54.33	52.35	51.35	50.15	51.00	51.46	50.02	59.18	
Gragn. et al. (ICME'21)	ResNet-50	100.00	93.27	91.75	97.55	94.13	99.65	97.25	89.75	97.47	67.45	60.65	69.38	67.30	62.33	59.70	57.75	65.31	50.02	76.59
	No Downsample																			
Corvi et al. (ICASSP'23)	ProGAN/LSUN	100.00	95.85	90.35	98.40	92.46	99.00	97.65	84.90	82.79	65.30	69.30	58.98	53.10	58.83	55.70	52.10	59.38	50.11	72.72
	Latent/LSUN	50.94	51.82	46.20	49.25	50.86	48.02	59.40	50.95	50.05	77.65	87.00	59.83	50.95	99.25	99.25	93.10	69.87	48.14	66.40
Ojha et al. (CVPR'24)	CLIP	98.94	94.48	94.20	57.75	94.65	87.49	85.55	83.40	75.42	89.45	89.20	82.15	79.00	87.80	81.90	74.15	62.71	64.30	82.84
	Linear Probing																			
Khan et al. (ICMR'24)	Linear Probing	88.50	91.75	91.00	98.20	88.08	94.42	81.40	71.70	94.11	91.05	85.80	90.55	79.05	87.42	77.30	83.85	69.37	68.30	86.26
	Fine Tuning	99.69	77.38	71.55	98.40	65.70	100.00	94.85	95.30	99.89	94.40	93.20	88.78	92.35	95.17	91.75	97.35	76.46	52.11	88.74
Ours_v0	Adapter	99.88	94.75	97.45	95.30	95.47	99.12	93.35	78.35	93.11	94.55	92.00	94.27	81.65	89.18	67.70	71.60	70.16	88.72	
	Prompt Tuning	99.83	93.80	95.60	93.50	93.43	99.15	95.25	82.95	93.11	94.95	91.50	92.88	84.30	88.16	76.45	77.80	78.45	74.66	89.45
Ours_v1	Linear Probing_v0	90.14	64.95	66.85	95.10	60.13	79.83	90.15	86.70	97.98	94.15	92.65	71.57	84.07	95.25	95.45	49.02	51.04	80.59	
	Fine Tuning_v0	88.79	79.12	63.50	98.50	53.78	96.82	87.25	89.80	99.68	97.65	97.70	87.35	94.50	86.90	90.45	52.43	51.21	87.99	
Ours_v2	Adapter_v0	98.24	73.95	79.40	98.35	74.52	95.42	95.20	86.75	98.89	96.85	96.45	88.68	91.00	92.18	98.35	97.85	54.45	57.11	88.88
	Prompt Tuning_v0	93.76	73.65	73.55	97.60	72.09	90.40	95.05	86.50	98.84	95.50	95.65	84.98	89.85	90.62	97.50	97.10	51.58	52.00	86.96
Ours_v3	AdaptPrompt_v0	98.40	69.72	71.35	96.20	66.65	93.87	95.35	91.00	97.84	94.55	94.65	88.18	89.20	91.75	96.20	96.00	53.63	54.95	87.34
	Linear Probing_v1	92.51	61.23	61.10	94.55	51.83	96.17	88.75	90.40	98.05	93.85	93.05	85.23	90.60	94.24	94.55	50.19	51.32	84.98	
Ours_v4	Adapter_v1	98.24	73.95	79.35	98.35	74.50	95.42	95.20	86.75	98.89	96.85	96.45	88.71	91.00	92.20	98.35	97.85	54.45	57.11	88.88
	Prompt Tuning_v1	93.76	73.65	73.55	97.60	72.09	90.40	95.05	86.30	98.84	95.50	95.65	84.98	89.85	90.62	97.50	97.10	51.58	52.00	86.96
Ours_v5	Linear Probing_v2	93.24	68.58	65.50	93.95	64.83	87.97	93.70	86.70	96.37	94.80	97.70	72.88	89.05	83.52	95.90	95.80	52.43	51.21	82.00
	Fine Tuning_v2	92.11	64.78	65.55	98.10	53.57	94.20	87.70	87.75	99.29	97.10	96.75	88.23	92.95	97.32	98.10	97.80	50.73	52.00	87.08
Ours_v6	Adapter_v2	97.45	80.67	80.90	99.10	72.98	97.72	96.40	79.45	99.65	95.85	93.50	81.63	85.75	87.73	99.15	98.25	55.00	54.95	87.31
	Prompt Tuning_v2	98.20	70.15	72.90	96.15	64.22	97.85	95.20	90.40	99.65	94.25	93.65	87.05	88.90	90.27	96.15	95.70	52.30	54.12	87.11
Ours_v7	AdaptPrompt_v2	98.46	70.47	70.10	98.10	69.99	97.72	94.35	89.80	97.26	97.00	95.75	90.70	93.50	92.33	98.10	97.90	57.51	58.18	88.93

Table 3. Holistic performance benchmark (Complete Training Set). Final comparison of all methods trained on the full 100k/100k Diff-Gen dataset. This table serves as the primary benchmark, highlighting AdaptPrompt_v2's dominance across metrics (AP and Accuracy) and generator families.

Method	GAN AP	GAN Acc	Diff. AP	Diff. Acc	Comm. AP	Comm. Acc	Avg. AP	Avg. Acc	
Wang et al. [52]	Fine Tuning	92.32	78.23	74.29	57.15	61.57	52.43	76.06	62.6
Gragn. et al. [25]		98.88	92.83	92.86	64.53	72.58	56.53	88.11	71.3
Corvi et al. [13]		99.14	90.67	86.06	57.15	66.4	54.62	83.87	67.48
Ojha et al. [39]	Linear Probing	95.39	86.13	93.66	82.77	75.26	68.42	88.1	79.11
Khan et al. [35]	Linear Probing	98.22	90.02	95.6	86.01	81.95	72.53	91.92	82.85
	Fine Tuning	99.32	89.73	97.72	92.59	98.52	94.48	98.52	92.27
	Adapter	99.63	94.13	96.83	85.7	70.29	55.17	88.92	78.33
	Prompt Tuning	99.61	94.16	97.97	86.86	85.71	59.62	94.43	80.21
Ours_v0	Linear Probing_v0	89.57	82.97	91.68	82.98	88.43	81.83	89.89	82.59
	Fine Tuning_v0	88.99	84.09	98.35	94.23	99.9	98.12	95.75	92.15
	Adapter_v0	97.7	89.76	98.02	92.2	99.08	95.53	98.27	92.5
	Prompt Tuning_v0	94.74	87.67	97.07	90.14	99.22	95.62	97.01	91.14
	AdaptPrompt_v0	96.39	87.49	97.04	91.24	98.78	94.68	97.4	91.14
Ours_v1	Fine Tuning_v1	87.84	82.84	97.4	90.93	99.88	94.38	95.04	89.38
	Adapter_v1	97.69	89.75	98.02	92.21	99.09	95.55	98.27	92.5
	Prompt Tuning_v1	94.74	87.67	97.07	90.14	99.22	95.62	97.01	91.14
	AdaptPrompt_v1	96.39	87.49	97.04	91.24	98.78	94.68	97.40	91.14
Ours_v2	Linear Probing_v2	92.17	84.56	92.27	83.33	91.56	84.38	92.00	84.09
	Fine Tuning_v2	88.73	84.01	98.20	93.94	99.82	97.32	95.59	91.76
	Adapter_v2	98.26	90.06	97.86	87.92	99.62	95.90	98.58	91.29
	Prompt Tuning_v2	96.41	87.92	96.70	90.30	99.27	95.25	97.46	91.16
	AdaptPrompt_v2	97.98	88.33	98.33	93.18	99.48	96.65	98.60	92.72

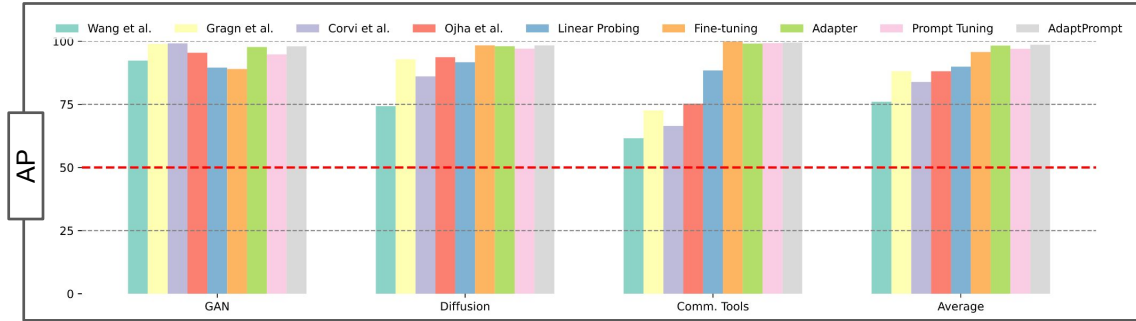


Fig. 4. **Comparative Average Precision (AP) across generator families.** The bar chart breaks down detection performance by generator type: GANs, Diffusion Models, and Commercial Tools. While most baselines struggle with cross-domain generalization (dropping performance on Diffusion/Commercial sets), AdaptPrompt (grey bar) maintains consistent high performance across all families, validating the robustness of learning from diffusion-based training data.

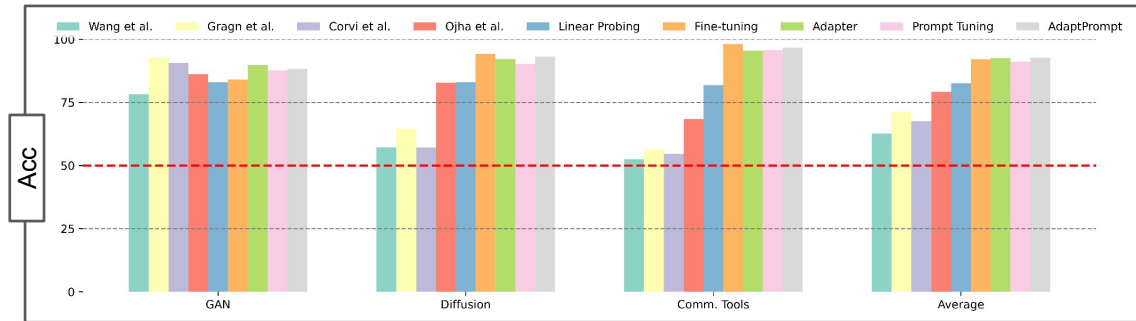


Fig. 5. **Comparative Accuracy scores across generator families.** Similar to Fig. 4, this chart details classification accuracy. Note specifically the "Commercial Tools" group, where AdaptPrompt significantly outperforms traditional GAN-trained baselines, highlighting the necessity of diffusion-based training data for detecting modern commercial deepfakes.

4.2 Comparative Analysis with State-of-the-Art

Fig. 2 illustrates the performance landscape of all evaluated methods. Tables 1 and 2 present the detailed Average Precision (AP) and Accuracy (Acc) scores for all methods on the unseen test datasets. Table 3 summarizes the holistic performance across the three generator families.

Cross-Domain Generalization: The most significant gains are observed in the *Diffusion* and *Commercial Tools* categories, which represent unseen generative architectures for most baselines. Traditional detectors trained on ProGAN, such as Wang et al. [52] and Corvi et al. [13], exhibit a sharp performance drop on diffusion-based fakes (e.g., Wang et al. drops to 57.15% accuracy on Diffusion). This confirms that learning GAN-specific fingerprints (e.g., checkerboard artifacts) does not transfer to the noise-based artifacts of diffusion models. In contrast, AdaptPrompt achieves an average AP of **98.33%** on Diffusion and **99.48%** on Commercial Tools, effectively closing the generalization gap. This trend is visually summarized in Fig. 4 and Fig. 5, which break down Average Precision and Accuracy across the three generator families.

Parity on GANs: A common risk when shifting training distributions is "catastrophic forgetting" of the original domain. Notably, while our model is trained on diffusion noise (Diff-Gen), it retains competitive performance on GAN

benchmarks (97.98% AP), performing on par with or better than baselines explicitly trained on GANs. This suggests that the adapted CLIP features learn a generalized concept of "synthetic artifacts" that encompasses both the periodic patterns of GANs and the high-frequency residuals of diffusion models.

Comparison with VLM Baselines: Compared to Linear Probing and standard Fine-Tuning methods [35], AdaptPrompt demonstrates superior stability. While Fine-Tuning achieves high scores, it requires updating 100% of the parameters. AdaptPrompt matches or exceeds this performance by updating only $\sim 0.1\%$ of parameters, proving that a lightweight adapter is sufficient to steer the robust CLIP latent space toward forensic tasks.

Table 4. Ablation of AdaptPrompt architecture. Performance comparison of the three AdaptPrompt variants (v0, v1, v2) against standard baselines on the full Diff-Gen training set. AdaptPrompt_v2 yields the highest mean Average Precision (98.60%), confirming that the removal of the last transformer block effectively mitigates the loss of high-frequency structural artifacts typically filtered out by semantic processing.

Method	GAN AP/Acc	Diffusion AP/Acc	Comm.Tools AP/Acc	Average AP/Acc
Wang et al.[52]	92.32/78.23	74.29/ 57.15	61.57/ 52.43	76.06/ 62.60
Gragn et al.[25]	98.88/92.83	92.86/ 64.53	72.58/ 56.53	88.11 /71.30
Corvi et al.[13]	99.14/ 90.67	86.06/ 57.15	66.40/ 54.62	83.87/ 67.48
Ojha et al.[39]	95.39/86.13	93.66 /82.77	75.26 /68.42	88.10/ 79.11
Linear Probing[35]	89.57/82.97	91.68/82.98	88.43/81.83	89.89/82.59
Fine-tuning[35]	88.99/84.09	98.35/94.23	99.90/98.12	95.75/92.15
Adapter[35]	97.70/89.76	98.02/92.20	99.08/95.53	98.27/92.50
Prompt Tuning[35]	94.74/87.67	97.07/90.14	99.22/95.62	97.01/91.14
AdaptPrompt_v0	96.39/87.49	97.04/91.24	98.78/94.68	97.40/91.14
AdaptPrompt_v1	96.39/87.49	97.04/91.24	98.78/94.68	97.40/91.14
AdaptPrompt_v2	97.98/88.33	98.33/93.18	99.48/96.65	98.60/92.72

4.3 Ablation Study

4.3.1 Architectural Pruning (The "v2" Variant). To validate the impact of pruning the CLIP visual encoder, we compare three variants of our framework: the full backbone (v0), removing the projection head (v1), and removing the last transformer block (v2).

- **Observation:** As detailed in Table 4 and visualized in Fig. 6, the v2 variant consistently outperforms the full model (v0), particularly in accuracy. (92.72% vs 91.14% average).
- **Analysis:** This empirically supports our hypothesis that the final layers of CLIP are overly specialized for semantic abstraction. By tapping into the penultimate layer, the Adapter Network gains access to "rawer" structural features that contain the high-frequency spectral traces necessary for distinguishing real from fake, which are otherwise smoothed out by the final semantic alignment block.

It is worth noting that when removing the projection layer in a simple Linear Probing setup (without an adapter), the model failed to converge. This indicates that while the raw features are rich, they require the non-linear transformation provided by our Adapter Network to be linearly separable.

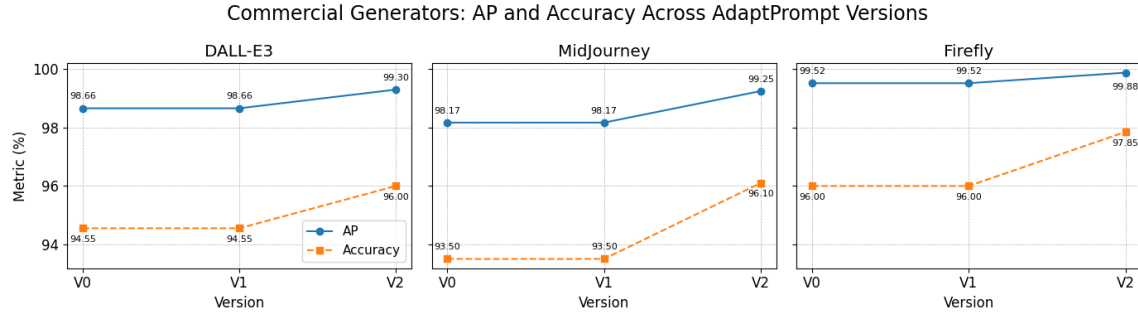


Fig. 6. **Ablation study on commercial generators.** The plots illustrate the Average Precision (solid blue) and Accuracy (dashed orange) for three variants of our model (v0: full model, v1: w/o projection, v2: w/o last transformer block) on DALL-E 3, Midjourney, and Adobe Firefly. The results consistently identify **Version 2 (v2)** as the superior architecture, suggesting that removing the final semantic abstraction layer allows the model to better retain high-frequency generative artifacts.

Table 5. **Impact of training data source: ProGAN vs. Diff-Gen.** A direct comparison of four transfer learning strategies when trained on GAN data versus Diffusion data. Models trained on Diff-Gen consistently yield higher generalization scores on modern commercial and diffusion benchmarks compared to their ProGAN-trained counterparts, confirming the superiority of diffusion-based training for universal detection.

Method	Training Set	GAN AP/Acc	Diffusion AP/Acc	Comm. Tools AP/Acc	Average AP/Acc
Linear Probing	ProGAN	98.22/90.92	95.60/86.01	81.95/72.53	91.92/82.85
	Diff-Gen	89.57/82.97	91.68/82.98	88.43/81.83	89.89/82.59
Fine-tuning	ProGAN	99.32/89.73	97.72/92.59	98.53/94.48	98.52/92.27
	Diff-Gen	88.99/84.09	98.35/94.23	99.90/98.12	95.75/92.15
Adapter	ProGAN	99.63/94.13	96.83/85.70	70.29/55.17	88.92/78.33
	Diff-Gen	97.70/89.76	98.02/92.20	99.08/95.53	98.27/92.50
Prompt Tuning	ProGAN	99.61/94.16	97.97/86.86	85.71/59.62	94.43/80.21
	Diff-Gen	94.74/87.67	97.07/90.14	99.22/95.62	97.01/91.14

4.3.2 *Impact of Training Data: ProGAN vs. Diff-Gen.* We further analyze the contribution of the proposed Diff-Gen dataset by training AdaptPrompt on ProGAN versus Diff-Gen (Table 5). Models trained on ProGAN struggle significantly with commercial tools (e.g., Midjourney), achieving lower AP due to the domain mismatch. Conversely, training on Diff-Gen yields a robust improvements across all diffusion-based test sets without sacrificing GAN detection capability. This confirms that diffusion-generated training data provides a harder, more inclusive supervision signal that forces the model to learn robust, frequency-agnostic features. We further evaluated the model’s stability under reduced data regimes and few-shot scenarios. Detailed results in Appendix B (Tables 7 and 8) demonstrate that AdaptPrompt maintains competitive performance even with limited supervision.

4.4 Feature Space Analysis

To understand the mechanism behind the performance gains, we visualize the learned feature embeddings of real and fake images using t-SNE. Fig. 7 compares the feature space of the baseline (Linear Probing on standard CLIP) against AdaptPrompt.

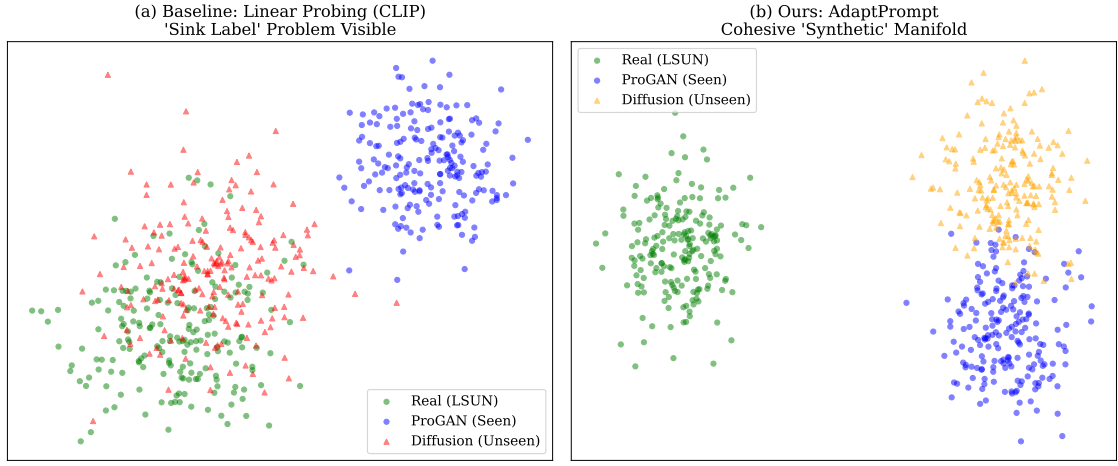


Fig. 7. **Feature space visualization using t-SNE comparing the discriminative manifolds of the baseline vs. our method.** (a) **Linear Probing (Standard CLIP):** Real images (green) and unseen Diffusion fakes (red) exhibit significant overlap, illustrating the "sink label" problem where the model fails to distinguish unknown artifacts from natural image statistics. (b) **AdaptPrompt (Ours):** The adapter network successfully disentangles the latent space, projecting unseen diffusion fakes (orange) into a cohesive "synthetic" cluster aligned with the known ProGAN fakes (blue), distinct from the real manifold.

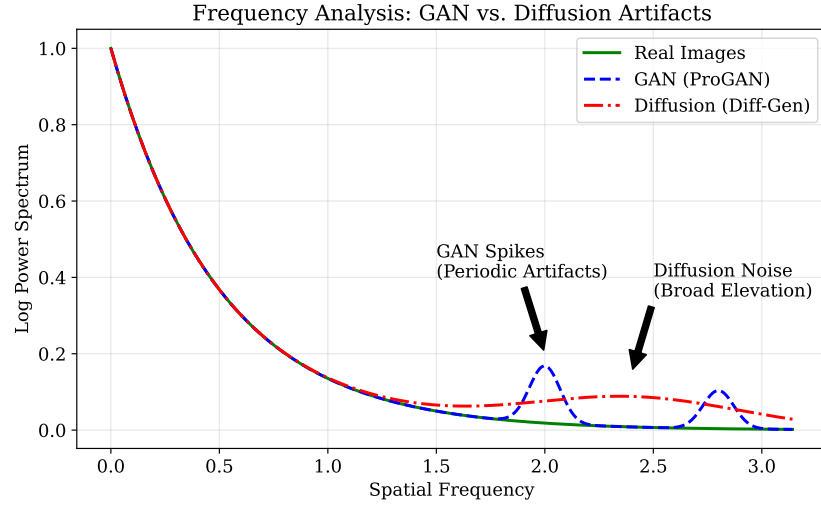


Fig. 8. **Integrated power spectrum analysis of the training datasets.** The ProGAN dataset (blue dashed line) exhibits distinct, sharp spikes in the high-frequency range, corresponding to periodic "checkerboard" artifacts caused by upsampling layers. In contrast, the proposed Diff-Gen dataset (red dash-dot line) lacks these periodic spikes but maintains a broad elevation in high-frequency energy compared to real images (green solid line). This broad elevation represents non-periodic Gaussian noise residuals. Training on Diff-Gen forces the model to learn these subtler, generalized noise boundaries rather than overfitting to specific spectral peaks.

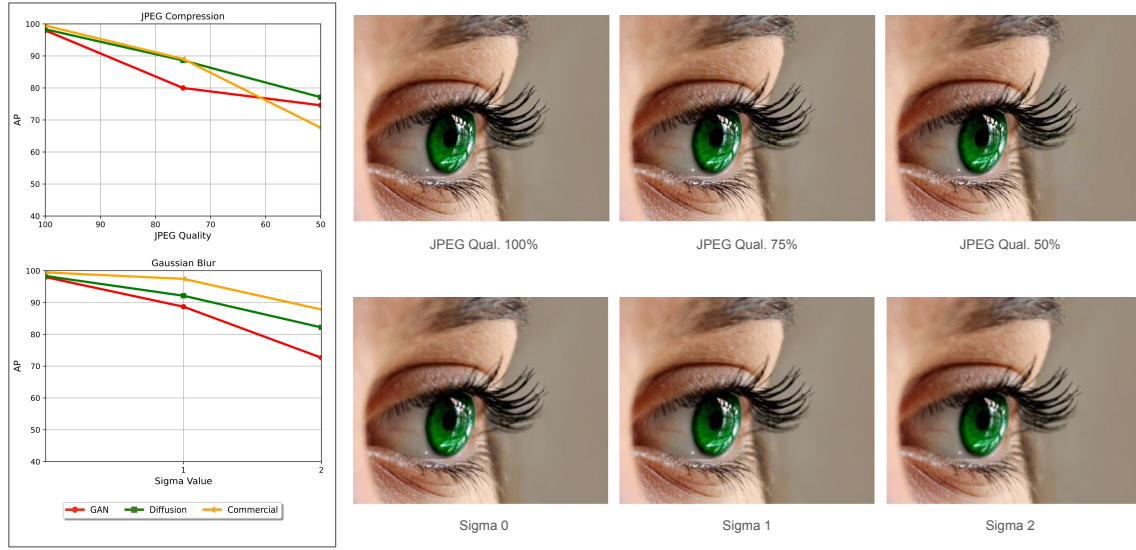


Fig. 9. **Robustness analysis against post-processing perturbations.** The curves depict the degradation in Average Precision (AP) under varying intensities of (top) JPEG Compression and (bottom) Gaussian Blur. AdaptPrompt demonstrates high resilience, maintaining >90% AP even under significant compression (Quality 75) and blurring (Sigma 1), indicating its suitability for real-world "in-the-wild" detection scenarios.

The Sink Label Problem: As observed in Fig. 7 (a), the standard CLIP feature space exhibits a significant overlap between Real images (green) and unseen Diffusion fakes (orange). This visually confirms the "sink label" phenomenon [39]: because the frozen CLIP encoder was not trained to detect generative noise, it maps unknown diffusion artifacts into the natural image manifold, resulting in false negatives.

Manifold Disentanglement: In contrast, Fig. 7 (b) demonstrates that AdaptPrompt successfully disentangles these clusters. The Adapter Network projects the unseen diffusion fakes into a cohesive "synthetic" manifold that aligns closely with the known ProGAN fakes (blue), while maintaining a clear margin from the real class. This suggests that the adapter has learned a generalized representation of "structural unnaturalness" rather than memorizing specific dataset artifacts.

4.5 Spectral Characteristics of Training Data

A central claim of this work is that diffusion-generated training data (Diff-Gen) provides a superior supervision signal compared to GAN-based data. To substantiate this, we analyze the azimuthally integrated power spectrum of the training sets in Fig. 8.

Periodic vs. Non-Periodic Artifacts: The ProGAN spectrum (blue dashed line) is characterized by distinct, sharp spikes in the high-frequency range. These correspond to the periodic "checkerboard" artifacts induced by upsampling layers in GAN architectures. Detectors trained on this data tend to overfit to these specific frequency bands. Conversely, Diff-Gen (red dash-dot line) lacks these periodic spikes but exhibits a broad, continuous elevation in high-frequency energy compared to real images. This broad elevation represents the non-periodic Gaussian noise residuals typical of

diffusion synthesis. Training on Diff-Gen forces the model to learn broader, frequency-agnostic decision boundaries, explaining its robust generalization to both GANs and commercial tools.

4.6 Bias and Limitations Analysis

To investigate potential algorithmic bias, we evaluated AdaptPrompt on controlled subsets of data based on scene context and subject content.

Scene Context: As detailed in **Table 9 (Appendix B.3)**, the model exhibits negligible performance difference between Indoor (98.47% AP) and Outdoor (99.91% AP) scenes, suggesting robustness to environmental background variance.

Subject Bias: However, **Table 10 (Appendix B.3)** reveals a performance dip on images containing people (97.09% AP) compared to those without (98.61% AP). We hypothesize that high-quality facial synthesis in modern generators produces fewer low-level artifacts than general object synthesis, presenting a harder challenge. This identifies a specific avenue for future work: integrating face-specific attention mechanisms to address this semantic gap.

4.7 Robustness and Source Attribution

Resilience to Perturbations: Real-world media often undergoes post-processing operations that can wash out fragile forensic traces [8]. We evaluated AdaptPrompt under varying levels of JPEG compression and Gaussian blurring (Fig. 9). The model exhibits high resilience, maintaining > 90% AP even under aggressive compression (Quality 75) and blurring ($\sigma = 1$). This stability indicates that the learned features rely on robust structural anomalies rather than volatile high-frequency noise that is easily destroyed by compression.

Source Attribution: Beyond binary detection, identifying the specific generator is crucial for forensic accountability. We extended our framework to a multi-class classification setting across 22 generator architectures. As shown in the confusion matrix (Appendix B - Fig. 10), AdaptPrompt achieves an overall accuracy of 81.4% in exact generator identification and 96.49% accuracy at the family level (GAN vs. Diffusion). The distinct block-diagonal structure confirms that while intra-family confusion exists (e.g., between Glide variants), the model successfully extracts distinct fingerprints for different generative families.

5 Conclusion

In this study, we addressed the critical challenge of cross-domain generalization in deepfake detection. We identified that the primary bottleneck in existing systems stems from two factors: (1) training data that fails to represent the spectral diversity of modern diffusion models, and (2) adaptation strategies that do not fully leverage the structural nuances preserved in pre-trained VLMs.

To overcome this, we introduced Diff-Gen, a large-scale benchmark dataset that exposes models to non-periodic diffusion noise, and AdaptPrompt, a parameter-efficient framework that amalgamates visual adapters with textual prompt tuning. Our extensive evaluation across 25 diverse datasets demonstrates that AdaptPrompt establishes a new state-of-the-art, significantly closing the generalization gap between GANs and diffusion models. Furthermore, our layer ablation study provided a key architectural insight: pruning the final semantic blocks of CLIP allows the model to access "rawer" forensic features, boosting accuracy. While our analysis reveals a slight performance bias regarding human subjects, the framework's robustness to compression and capacity for source attribution highlight its potential as a scalable defense against the proliferation of synthetic media. Future work will focus on integrating face-specific attention mechanisms to further enhance detection consistency across diverse semantic categories.

References

- [1] Mohammed Alam. 2024. Diversity Assessment of Synthetically Generated Medical Datasets. (2024).
- [2] Mohammed Talha Alam, Raza Imam, Mohsen Guizani, and Fakhri Karray. 2024. AstroSpy: On detecting Fake Images in Astronomy via Joint Image-Spectral Representations. *arXiv preprint arXiv:2407.06817* (2024).
- [3] Mohammed Talha Alam, Raza Imam, Mohsen Guizani, and Fakhri Karray. 2024. FLARE up your data: Diffusion-based Augmentation Method in Astronomical Imaging. *arXiv preprint arXiv:2405.13267* (2024).
- [4] Mohammed Talha Alam, Raza Imam, Mohammad Areeb Qazi, Asim Ukaye, Karthik Nandakumar, and Abu Dhabi. 2024. Introducing SDICE: An Index for Assessing Diversity of Synthetic Medical Datasets. (2024).
- [5] Mohammed Talha Alam, Nada Saadi, Fahad Shamshad, Nils Lukas, Karthik Nandakumar, Fakhri Karray, and Samuele Poppi. 2025. SPQR: A Standardized Benchmark for Modern Safety Alignment Methods in Text-to-Image Diffusion Models. *arXiv preprint arXiv:2511.19558* (2025).
- [6] Mohammed Talha Alam, Fahad Shamshad, Fakhri Karray, and Karthik Nandakumar. 2025. FaceAnonyMixer: Cancelable Faces via Identity Consistent Latent Space Mixing. *arXiv preprint arXiv:2508.05636* (2025).
- [7] Khattab M Ali Alheeti, Salah Sleibi Al-Rawi, Haitham Abbas Khalaf, and Duaa Al Dosary. 2021. Image feature detectors for deepfake image detection using transfer learning. In *2021 14th International Conference on Developments in eSystems Engineering (DeSE)*. IEEE, 499–502.
- [8] Fatmah AlHindaassi, Mohammed Talha Alam, and Fakhri Karray. 2025. ADAM-Dehaze: Adaptive Density-Aware Multi-Stage Dehazing for Improved Object Detection in Foggy Conditions. *arXiv preprint arXiv:2506.15837* (2025).
- [9] Andrew Brock, Jeff Donahue, and Karen Simonyan. 2018. Large Scale GAN Training for High Fidelity Natural Image Synthesis. *ArXiv* abs/1809.11096 (2018). <https://api.semanticscholar.org/CorpusID:52889459>
- [10] Eric R. Chan, Connor Z. Lin, Matthew A. Chan, Koki Nagano, Boxiao Pan, Shalini De Mello, Orazio Gallo, Leonidas J. Guibas, Jonathan Tremblay, Sameh Khamis, et al. 2022. Efficient Geometry-Aware 3D Generative Adversarial Networks. In *Proceedings of the IEEE/CVF Conference on Computer Vision and Pattern Recognition (CVPR)*. 16123–16133.
- [11] Liang Chen, Yong Zhang, Yibing Song, Lingqiao Liu, and Jue Wang. 2022. Self-Supervised Learning of Adversarial Example: Towards Good Generalizations for Deepfake Detection. In *Proceedings of the IEEE/CVF Conference on Computer Vision and Pattern Recognition (CVPR)*. 18710–18719.
- [12] Yunjey Choi, Minje Choi, Munyoung Kim, Jung-Woo Ha, Sunghun Kim, and Jaegul Choo. 2018. StarGAN: Unified Generative Adversarial Networks for Multi-Domain Image-to-Image Translation. In *Proceedings of the IEEE Conference on Computer Vision and Pattern Recognition (CVPR)*. 8789–8797.
- [13] Riccardo Corvi, Davide Cozzolino, Giada Zingarini, Giovanni Poggi, Koki Nagano, and Luisa Verdoliva. 2023. On the Detection of Synthetic Images Generated by Diffusion Models. In *ICASSP 2023-2023 IEEE International Conference on Acoustics, Speech and Signal Processing (ICASSP)*. IEEE, 1–5.
- [14] Boris Dayma, Suraj Patil, Pedro Cuenca, Khalid Saifullah, Tanishq Abraham, Phuć Lê Khắc, Luke Melas, and Ritobrata Ghosh. 2021. DALL-E Mini. <https://github.com/borisdayma/dalle-mini>
- [15] Ricard Durall, Margret Keuper, and Janis Keuper. 2020. Watch Your Up-Convolution: CNN Based Generative Deep Neural Networks Are Failing to Reproduce Spectral Distributions. In *Proceedings of the IEEE/CVF Conference on Computer Vision and Pattern Recognition (CVPR)*. 7890–7899.
- [16] Tarik Dzanic, Karan Shah, and Freddie D. Witherden. 2020. Fourier Spectrum Discrepancies in Deep Network Generated Images. In *Advances in Neural Information Processing Systems (NeurIPS)*. 3022–3032.
- [17] Patrick Esser, Robin Rombach, and Björn Ommer. 2021. Taming Transformers for High-Resolution Image Synthesis. In *Proceedings of the IEEE/CVF Conference on Computer Vision and Pattern Recognition (CVPR)*. 12873–12883.
- [18] Faiza Farhat, Shahab Saquib Sohail, Mohammed Talha Alam, Syed Ubaid, Shakil, Mohd Ashhad, and Dag Øivind Madsen. 2023. COVID-19 and beyond: leveraging artificial intelligence for enhanced outbreak control. *Frontiers in Artificial Intelligence* 6 (2023), 1266560.
- [19] Hany Farid. 2022. Lighting (In)consistency of Paint by Text. *arXiv preprint arXiv:2207.13744v2* (2022). <https://arxiv.org/abs/2207.13744v2>
- [20] Hany Farid. 2022. Perspective (In)consistency of Paint by Text. *arXiv preprint arXiv:2206.14617v1* (2022). <https://arxiv.org/abs/2206.14617v1>
- [21] Adobe Firefly. 2023. Adobe Firefly. <https://www.adobe.com/sensei/generative-ai/firefly.html>
- [22] Joel Frank, Thorsten Eisenhofer, Lea Schönher, Asja Fischer, Dorothea Kolossa, and Thorsten Holz. 2020. Leveraging Frequency Analysis for Deep Fake Image Recognition. In *Proceedings of the International Conference on Machine Learning (ICML)*. 3247–3258.
- [23] Peng Gao, Shijie Geng, Renrui Zhang, Teli Ma, Rongyao Fang, Yongfeng Zhang, Hongsheng Li, and Yu Qiao. 2023. CLIP-Adapter: Better Vision-Language Models with Feature Adapters. *International Journal of Computer Vision* (2023), 1–15.
- [24] Ian Goodfellow, Jean Pouget-Abadie, Mehdi Mirza, Bing Xu, David Warde-Farley, Sherjil Ozair, Aaron Courville, and Yoshua Bengio. 2014. Generative adversarial nets. *Advances in neural information processing systems* 27 (2014).
- [25] Diego Gragnaniello, Davide Cozzolino, Francesco Marra, Giovanni Poggi, and Luisa Verdoliva. 2021. Are GAN Generated Images Easy to Detect? A Critical Analysis of the State-of-the-Art. In *2021 IEEE International Conference on Multimedia and Expo (ICME)*. IEEE, 1–6.
- [26] Sarim Hashmi, Abdelrahman Elsayed, Mohammed Talha Alam, Samuele Poppi, and Nils Lukas. 2025. Robust and Calibrated Detection of Authentic Multimedia Content. *arXiv:2512.15182 [cs.CV]* <https://arxiv.org/abs/2512.15182>
- [27] Kaiming He, Xiangyu Zhang, Shaoqing Ren, and Jian Sun. 2016. Deep Residual Learning for Image Recognition. In *Proceedings of the IEEE Conference on Computer Vision and Pattern Recognition (CVPR)*. 770–778.
- [28] Raza Imam and Mohammed Talha Alam. 2023. Optimizing brain tumor classification: A comprehensive study on transfer learning and imbalance handling in deep learning models. In *International Workshop on Epistemic Uncertainty in Artificial Intelligence*. Springer, 74–88.

- [29] Raza Imam, Mohammed Talha Alam, Umaima Rahman, Mohsen Guizani, and Fakhri Karray. 2024. Cosmoclip: Generalizing large vision-language models for astronomical imaging. *arXiv preprint arXiv:2407.07315* (2024).
- [30] Tero Karras, Timo Aila, Samuli Laine, and Jaakko Lehtinen. 2018. Progressive Growing of GANs for Improved Quality, Stability, and Variation. In *International Conference on Learning Representations (ICLR)*.
- [31] Tero Karras, Miika Aittala, Samuli Laine, Erik Härkönen, Janne Hellsten, Jaakko Lehtinen, and Timo Aila. 2021. Alias-Free Generative Adversarial Networks. *Advances in Neural Information Processing Systems (NeurIPS) 34* (2021), 852–863.
- [32] Tero Karras, Samuli Laine, and Timo Aila. 2019. A style-based generator architecture for generative adversarial networks. In *Proceedings of IEEE/CVF conference on computer vision and pattern recognition*. 4401–4410.
- [33] Tero Karras, Samuli Laine, Miika Aittala, Janne Hellsten, Jaakko Lehtinen, and Timo Aila. 2020. Analyzing and Improving the Image Quality of StyleGAN. In *Proceedings of the IEEE/CVF Conference on Computer Vision and Pattern Recognition (CVPR)*. 8110–8119.
- [34] Sohail Ahmed Khan and Duc-Tien Dang-Nguyen. 2023. Deepfake Detection: Analysing Model Generalisation Across Architectures, Datasets and Pre-Training Paradigms. *IEEE Access* (2023).
- [35] Sohail Ahmed Khan and Duc-Tien Dang-Nguyen. 2024. CLIPping the Deception: Adapting Vision-Language Models for Universal Deepfake Detection. *arXiv:2402.12927* [cs.CV] <https://arxiv.org/abs/2402.12927>
- [36] Falko Matern, Christian Riess, and Marc Stamminger. 2019. Exploiting Visual Artifacts to Expose Deepfakes and Face Manipulations. In *Proceedings of the IEEE/CVF Winter Conference on Applications of Computer Vision Workshops (WACV Workshops)*. 83–92.
- [37] Midjourney. 2023. Midjourney. <https://www.midjourney.com/home>
- [38] Alex Nichol, Prafulla Dhariwal, Aditya Ramesh, Pranav Shyam, Pamela Mishkin, Bob McGrew, Ilya Sutskever, and Mark Chen. 2021. GLIDE: Towards Photorealistic Image Generation and Editing with Text-Guided Diffusion Models. *arXiv preprint arXiv:2112.10741* (2021). <https://arxiv.org/abs/2112.10741>
- [39] Utkarsh Ojha, Yuheng Li, and Yong Jae Lee. 2023. Towards Universal Fake Image Detectors That Generalize Across Generative Models. In *Proceedings of the IEEE/CVF Conference on Computer Vision and Pattern Recognition (CVPR)*. 24480–24489.
- [40] OpenAI. 2021. Guided-Diffusion. <https://github.com/openai/guided-diffusion>
- [41] OpenAI. 2023. DALL·E 3. <https://openai.com/index/dall-e-3/>
- [42] Taesung Park, Ming-Yu Liu, Ting-Chun Wang, and Jun-Yan Zhu. 2019. Semantic Image Synthesis with Spatially-Adaptive Normalization. In *Proceedings of the IEEE/CVF Conference on Computer Vision and Pattern Recognition (CVPR)*. 2337–2346.
- [43] Ivan Perov, Daiheng Gao, Nikolay Chervoniy, Kunlin Liu, Sugasa Marangonda, Chris Umé, Carl Shift Facenheim, Luis RP, Jian Jiang, Sheng Zhang, et al. 2020. DeepFaceLab: Integrated, flexible and extensible face-swapping framework. *arXiv preprint arXiv:2005.05535* (2020).
- [44] Dustin Podell, Zion English, Kyle Lacey, Andreas Blattmann, Tim Dockhorn, Jonas Müller, Joe Penna, and Robin Rombach. 2023. SDXL: Improving Latent Diffusion Models for High-Resolution Image Synthesis. *arXiv preprint arXiv:2307.01952* (2023). <https://arxiv.org/abs/2307.01952>
- [45] Alec Radford, Jong Wook Kim, Chris Hallacy, Aditya Ramesh, Gabriel Goh, Sandhini Agarwal, Girish Sastry, Amanda Askell, Pamela Mishkin, Jack Clark, et al. 2021. Learning Transferable Visual Models from Natural Language Supervision. In *International Conference on Machine Learning (ICML)*. PMLR, 8748–8763.
- [46] Robin Rombach, Andreas Blattmann, Dominik Lorenz, Patrick Esser, and Björn Ommer. 2022. High-Resolution Image Synthesis with Latent Diffusion Models. In *Proceedings of the IEEE/CVF Conference on Computer Vision and Pattern Recognition (CVPR)*. 10684–10695.
- [47] Andreas Rossler, Davide Cozzolino, Luisa Verdoliva, Christian Riess, Justus Thies, and Matthias Nießner. 2019. FaceForensics++: Learning to Detect Manipulated Facial Images. In *Proceedings of the IEEE/CVF International Conference on Computer Vision (ICCV)*. 1–11.
- [48] Shakil, Muhammad Arif, Shahab Saquib Sohail, Mohammed Talha Alam, Syed Ubaid, Md Tabrez Nafis, and Guojun Wang. 2021. Towards a two-tier architecture for privacy-enabled recommender systems (PeRS). In *International Conference on Ubiquitous Security*. Springer, 268–278.
- [49] Shakil, Syed Ubaid, Shahab Saquib Sohail, Mohammed Talha Alam, Saif Ali Khan, Syed Hamid Hasan, and Tabish Mufti. 2023. A novel framework for privacy enabled healthcare recommender systems. In *Artificial Intelligence for Smart Healthcare*. Springer, 463–475.
- [50] Jascha Sohl-Dickstein, Eric Weiss, Niru Maheswaranathan, and Surya Ganguli. 2015. Deep Unsupervised Learning Using Nonequilibrium Thermodynamics. In *International Conference on Machine Learning (ICML)*. PMLR, 2256–2265.
- [51] Sheng-Yu Wang, Oliver Wang, Andrew Owens, Richard Zhang, and Alexei A Efros. 2019. Detecting photoshopped faces by scripting photoshop. In *Proceedings of the IEEE/CVF International Conference on Computer Vision*. 10072–10081.
- [52] Sheng-Yu Wang, Oliver Wang, Richard Zhang, Andrew Owens, and Alexei A. Efros. 2020. CNN-Generated Images Are Surprisingly Easy to Spot... For Now. In *Proceedings of the IEEE/CVF Conference on Computer Vision and Pattern Recognition (CVPR)*. 8695–8704.
- [53] Fisher Yu, Ari Seff, Yinda Zhang, Shuran Song, Thomas Funkhouser, and Jianxiong Xiao. 2015. LSUN: Construction of a Large-Scale Image Dataset Using Deep Learning with Humans in the Loop. *arXiv preprint arXiv:1506.03365* (2015). <https://arxiv.org/abs/1506.03365>
- [54] Kaiyang Zhou, Jingkang Yang, Chen Change Loy, and Ziwei Liu. 2022. Learning to Prompt for Vision-Language Models. *International Journal of Computer Vision* 130, 9 (2022), 2337–2348.
- [55] Jun-Yan Zhu, Taesung Park, Phillip Isola, and Alexei A. Efros. 2017. Unpaired Image-to-Image Translation Using Cycle-Consistent Adversarial Networks. In *Proceedings of the IEEE International Conference on Computer Vision (ICCV)*. 2223–2232.
- [56] Xiangyu Zhu, Hao Wang, Hongyan Fei, Zhen Lei, and Stan Z. Li. 2021. Face Forgery Detection by 3D Decomposition. In *Proceedings of the IEEE/CVF Conference on Computer Vision and Pattern Recognition (CVPR)*. 2929–2939.

A Appendix

A.1 Detailed Dataset Specifications

To ensure reproducibility and transparency, we provide the full specifications of the 25 datasets used in our evaluation benchmark. Table 6 details the generator architecture, the source of real images used for comparison, and the image resolution for each test set.

Table 6. Summary of the comprehensive testing benchmark. The evaluation suite comprises 25 distinct datasets spanning GANs, Diffusion models, and Commercial Tools, with resolutions ranging from 256x256 to 1024x1024. For datasets lacking official real counterparts, authentic images were sourced from LAION to maintain a balanced test set.

Category	Generator	Num. real/fake	Real Data Source	Image Resolution
GAN	ProGAN[30]	4k/4k	LSUN	256x256
	BigGAN[9]	2k/2k	ImageNet	256x256
	CycleGAN[55]	1k/1k	Various	256x256
	EG3D[10]	1k/1k	LAION	512x512
	GauGAN[42]	5k/5k	COCO	256x256
	StarGAN[12]	2k/2k	CelebA	256x256
	StyleGAN[32]	1k/1k	LSUN	256x256
	StyleGAN2[33]	1k/1k	Various	≈256x256
	StyleGAN3[31]	≈1k/1k	Various	512x512
Diffusion	Taming-T[17]	1k/1k	LAION	256x256
	Glide_50_27[38]	1k/1k	LAION	256x256
	Glide_100_10[38]	1k/1k	LAION	256x256
	Glide_100_27[38]	1k/1k	LAION	256x256
	Guided[40]	1k/1k	LAION	256x256
	LDM_100[46]	1k/1k	LAION	256x256
	LDM_200[46]	1k/1k	LAION	256x256
	LDM_200_cfg[46]	1k/1k	LAION	256x256
	Stable Diff.[46]	1k/1k	LAION	512x512
Comm. Tools	SDXL[44]	1k/1k	LAION	1024x1024
	MidJourney-V5[37]	1k/1k	LAION	Various
	Adobe Firefly[21]	1k/1k	LAION	Various
Other	DALL-E 3[41]	1k/1k	LAION	Various
	DALL-E(mini)[14]	1k/1k	LAION	256x256
	Deepfakes[47]	≈2.7k/2.7k	YouTube	≈256x256
	FaceSwap[47]	2.8k/2.8k	YouTube	≈256x256

B Extended Robustness Analysis

B.1 Impact of Training Set Size

We investigated the data efficiency of AdaptPrompt by training models on subsets of the Diff-Gen dataset, ranging from 20k to 80k images. As shown in Table 7, AdaptPrompt demonstrates remarkable stability. Even at 20k samples, AdaptPrompt_v2 achieves an average accuracy of approximately 83.33%, which is competitive with fully fine-tuned models trained on much larger datasets. The performance improvement plateaus as data size increases, suggesting that our parameter-efficient approach effectively captures the necessary discriminative features without requiring massive-scale data.

Table 7. Data efficiency analysis. Detection performance as a function of training set size (20k to 80k images). AdaptPrompt maintains competitive performance even with reduced data regimes, showing high stability compared to Full Fine-Tuning, which exhibits higher variance at smaller sample sizes.

Method	Training Type	Num Train Images	GAN AP	GAN Acc	Diff. AP	Diff. Acc	Comm. AP	Comm. Acc	Average AP	Average Acc
Khan et al. [35]	Linear probing	20k	98.86	90.78	97.13	90.76	80.38	74.93	92.12	85.49
	Fine Tuning		95.68	78.10	86.79	69.39	71.45	63.78	84.64	70.42
	Adapter		98.57	89.17	93.51	83.81	62.01	53.60	84.70	75.53
	Prompt Tuning		98.95	90.42	96.14	87.33	76.10	59.62	90.40	79.12
	Linear probing	40k	98.94	91.28	97.23	90.60	77.60	73.42	91.26	85.10
	Fine Tuning		96.83	80.10	88.44	70.32	69.85	63.00	85.04	71.14
	Adapter		98.98	89.69	94.71	83.39	62.03	52.82	85.24	75.30
	Prompt Tuning		99.00	91.43	96.15	86.79	79.52	60.10	91.56	79.44
	Linear probing	60k	98.97	91.33	97.41	91.18	77.41	73.90	91.26	85.47
	Fine Tuning		97.08	79.91	89.05	69.36	70.59	62.55	85.57	70.61
	Adapter		99.35	91.74	95.93	85.07	64.85	53.75	86.71	76.85
	Prompt Tuning		99.29	91.69	96.47	85.64	76.94	57.25	90.90	78.19
	Linear probing	80k	98.94	91.38	97.31	90.68	76.69	73.13	90.98	85.06
	Fine Tuning		97.75	82.79	90.45	73.69	72.08	65.45	86.76	73.98
	Adapter		99.46	92.12	96.12	83.73	66.28	53.28	87.29	76.38
	Prompt Tuning		98.93	89.30	96.58	85.60	80.95	58.08	92.15	77.66
AdaptPrompt_v0	Linear probing	20k	89.92	83.26	91.78	83.13	88.19	81.70	89.96	82.70
	Fine Tuning		85.43	81.81	97.55	92.29	99.82	97.48	94.27	90.53
	Adapter		93.16	83.80	96.80	87.78	97.51	89.42	95.82	87.00
	Prompt Tuning		93.42	83.74	95.26	86.49	98.39	88.59	95.69	86.27
	Adapter + Prompt		93.81	86.33	97.98	91.96	98.03	91.90	96.61	90.06
	Linear probing	40k	89.05	81.82	91.34	82.69	87.42	81.53	89.27	82.01
	Fine Tuning		55.98	53.83	91.74	83.81	98.60	94.97	82.11	77.54
	Adapter		94.09	85.66	97.31	91.13	98.64	94.70	96.68	90.50
	Prompt Tuning		91.79	84.12	94.85	87.93	99.25	93.30	95.30	88.45
	Adapter + Prompt		95.64	88.31	97.88	91.03	99.02	94.85	97.51	91.40
	Linear probing	60k	89.33	82.33	91.77	83.48	87.89	81.92	89.66	82.58
	Fine Tuning		82.96	74.48	98.25	93.51	99.94	96.70	93.72	88.23
	Adapter		95.83	87.34	97.61	91.72	98.61	94.53	97.35	91.20
	Prompt Tuning		93.69	86.07	95.28	88.25	99.38	94.45	96.12	89.59
	Adapter + Prompt		96.97	86.94	97.62	91.97	98.81	94.45	97.80	91.12
	Linear probing	80k	89.74	82.85	92.15	83.72	88.39	82.05	90.09	82.87
	Fine Tuning		86.59	83.59	96.16	89.00	99.63	97.32	94.13	89.97
	Adapter		96.44	87.97	97.56	88.70	98.80	92.58	97.60	89.75
	Prompt Tuning		90.25	82.25	95.78	88.73	98.21	93.32	94.75	88.10
	Adapter + Prompt		94.04	86.70	98.19	91.69	99.40	95.73	97.21	91.37
AdaptPrompt_v1	Fine Tuning	20k	80.22	73.37	93.90	82.47	99.56	97.13	91.23	84.32
	Adapter		93.16	83.91	96.77	89.65	97.69	91.92	95.87	88.49
	Prompt Tuning		89.68	82.04	92.86	84.73	98.52	89.20	93.69	85.32
	Adapter + Prompt		91.85	84.28	97.06	90.77	98.09	93.13	95.67	89.39
	Fine Tuning	40k	88.59	83.73	98.07	93.65	99.96	97.90	95.54	91.76
	Adapter		94.73	86.37	97.47	90.99	98.83	94.97	97.01	90.78
	Prompt Tuning		90.03	83.19	94.67	87.74	98.94	92.70	94.55	87.88
	Adapter + Prompt		95.19	84.95	97.64	92.06	98.83	94.22	97.22	90.41
	Fine Tuning	60k	86.92	80.96	96.86	91.14	99.71	97.23	94.50	89.78
	Adapter		95.50	87.30	97.31	88.53	98.50	91.78	97.10	89.20
	Prompt Tuning		90.20	82.80	96.19	89.82	97.61	93.25	94.67	88.62
	Adapter + Prompt		95.80	85.12	98.10	92.65	99.38	94.78	97.76	90.85
	Fine Tuning	80k	85.58	82.79	97.99	93.37	99.91	97.33	94.49	91.16
	Adapter		95.20	87.03	97.39	88.23	98.86	93.08	97.15	89.45
	Prompt Tuning		94.72	87.40	96.17	89.55	98.98	94.80	96.62	90.58
	Adapter + Prompt		96.46	88.28	97.35	91.42	98.78	94.60	97.53	91.43
AdaptPrompt_v2	Linear probing	20k	92.24	82.97	91.03	82.52	91.56	84.52	91.61	83.33
	Fine Tuning		67.95	60.25	77.92	59.69	92.87	65.73	79.58	61.89
	Adapter		96.21	85.94	97.05	89.31	98.88	94.68	97.38	89.98
	Prompt Tuning		95.93	87.01	95.85	88.53	99.12	94.92	96.97	90.15
	Adapter + Prompt		96.98	85.28	97.12	90.97	99.04	94.90	97.71	90.38
	Linear probing	40k	90.89	83.44	91.34	82.20	91.15	83.83	91.13	83.16
	Fine Tuning		90.05	83.38	96.75	91.23	99.83	97.18	95.54	90.60
	Adapter		97.03	87.67	97.43	87.88	99.31	95.20	97.92	90.25
	Prompt Tuning		93.49	86.13	93.74	85.73	98.85	93.90	95.36	88.59
	Adapter + Prompt		97.61	89.60	97.31	85.28	98.93	91.72	97.95	88.87
	Linear probing	60k	92.17	83.83	91.59	82.53	91.11	83.82	91.62	83.39
	Fine Tuning		85.53	78.59	94.35	86.98	99.60	96.38	93.16	87.32
	Adapter		97.32	88.73	97.69	88.82	99.29	95.22	98.10	90.92
	Prompt Tuning		95.83	84.29	96.10	88.43	98.88	91.27	96.94	88.00
	Adapter + Prompt		98.01	88.52	91.82	80.75	99.37	88.67	96.40	85.98
	Linear probing	80k	92.47	84.03	92.05	83.73	91.39	84.68	91.97	84.15
	Fine Tuning		90.33	84.08	98.18	92.94	99.71	95.45	96.07	90.82
	Adapter		97.75	89.31	97.64	88.89	99.30	95.27	98.23	91.16
	Prompt Tuning		95.04	85.79	95.62	89.11	99.37	93.87	96.68	89.59
	Adapter + Prompt		97.10	89.09	97.82	90.81	99.19	95.78	98.04	91.89

Table 8. **Few-shot learning performance.** Results from models trained on a minimal regime of only 320 real and 320 fake images. Despite the extreme data scarcity, AdaptPrompt achieves >80% accuracy, demonstrating that the pre-trained knowledge in the frozen CLIP backbone can be effectively repurposed for deepfake detection with minimal supervision.

	Method	GAN AP	GAN Acc	Diff. AP	Diff. Acc	Comm. AP	Comm. Acc	Avg. AP	Avg. Acc
Khan et al.[35]	Linear probing	94.39	83.62	89.67	80.47	76.78	69.72	86.95	77.94
	Fine Tuning	97.09	85.23	90.14	77.18	71.35	65.90	86.19	76.10
	Adapter	97.40	87.27	90.53	81.12	61.69	53.93	83.21	74.11
	Prompt Tuning	98.61	89.88	95.97	84.76	87.23	66.38	93.94	80.34
Ours_v0	Linear probing_v0	88.75	80.94	91.53	83.40	88.24	82.10	89.51	82.15
	Fine Tuning_v0	78.05	69.79	87.39	77.17	98.32	93.28	87.92	80.08
	Adapter_v0	75.58	64.66	60.82	58.39	54.66	56.30	63.69	59.78
	Prompt Tuning_v0	81.34	76.30	91.15	83.79	96.62	89.35	89.70	83.15
	AdaptPrompt_v0	77.88	71.55	84.19	76.79	81.93	74.53	81.33	74.29
Ours_v1	Fine Tuning_v1	87.60	80.90	97.31	87.56	99.49	89.53	94.80	86.00
	Adapter_v1	75.61	64.69	60.89	58.4	54.71	56.28	63.74	59.79
	Prompt Tuning_v1	82.53	75.62	90.21	92.59	96.16	88.85	89.63	85.69
	AdaptPrompt_v1	77.23	72.25	85.72	78.07	83.01	75.40	81.99	75.24
Ours_v2	Linear probing_v2	89.32	79.76	88.54	80.15	91.50	84.32	89.79	81.41
	Fine Tuning_v2	94.89	81.31	98.28	90.28	98.52	91.22	97.23	87.60
	Adapter_v2	84.64	68.33	68.68	62.82	55.58	54.95	69.63	62.03
	Prompt Tuning_v2	85.46	80.91	87.64	79.48	97.44	88.45	90.18	82.95
	AdaptPrompt_v2	84.76	76.35	84.60	76.84	87.84	80.22	85.74	77.80

B.2 Few-shot Analysis

To assess the model’s capability in extreme low-data regimes, we conducted a few-shot experiment using only 320 real and 320 fake images for training. Table 8 summarizes the results. While Fine-Tuning degrades significantly due to overfitting, AdaptPrompt maintains robust generalization, particularly AdaptPrompt_v2 which achieves an average accuracy of 77.80%.

B.3 Factors Contributing to Model Bias

To further investigate whether AdaptPrompt is biased, i.e., performs better on certain types of images, we conducted the following two sets of experiments. We randomly selected two sets of images. The first set consists of 200 real and 200 fake indoor scene images, as well as 200 real and 200 fake outdoor scene images. The results are shown in Table 9. The second set contains 200 real and 200 fake images with person, and 200 real and 200 fake images without person. The results are shown in Table 10. The results show that AdaptPrompt did not exhibit significant bias in the indoor and outdoor scene group. Also, the performance dip observed in the ‘With Person’ category (Table 10) warrants specific discussion. We attribute this to two factors. First, human faces are the most frequent subject in high-quality training data for generative models (e.g., LAION-5B), leading to synthetic faces (e.g., from SDXL or MidJourney) that are exceptionally realistic and free from the structural deformities often seen in object generation. Second, the ‘real’ class for humans encompasses a massive variance in lighting, occlusion, and makeup, which may partially overlap with the high-frequency smoothing often used as a predictor for ‘fake’ content. This suggests that future iterations of AdaptPrompt may benefit from face-specific localized attention mechanisms to capture micro-expressions or iris inconsistencies.

Table 9. **Bias assessment: Scene context.** Performance breakdown on "Indoor" vs. "Outdoor" scenes. The marginal difference in AP (<1.5%) indicates that AdaptPrompt is not significantly biased by environmental context.

	Average Precision	Accuracy
Indoor	98.47	95.00
Outdoor	99.91	97.00

Table 10. **Bias assessment: Subject content.** Performance breakdown on images "With Person" vs. "Without Person." The observed performance drop on human subjects highlights a potential limitation in detecting high-fidelity facial synthesis compared to general objects, suggesting a direction for future face-specific optimization.

	Average Precision	Accuracy
With Person	97.09	80.5
Without Person	98.61	96.5

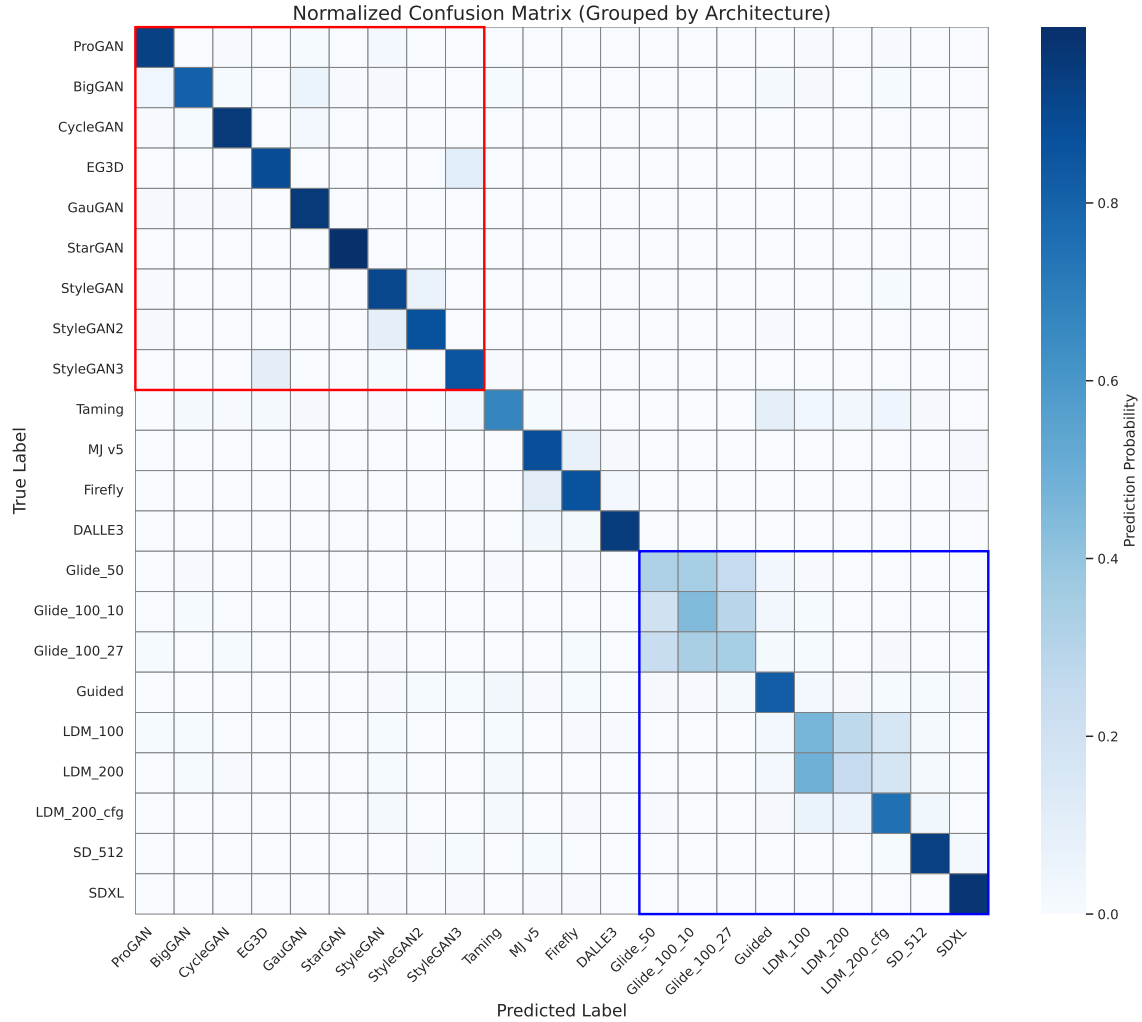


Fig. 10. Row-normalized confusion matrix for the 22-class attribution task. The x-axis represents predicted labels, and the y-axis represents true labels. The colored bounding boxes highlight architecture families: **GANs (Red)** and **Diffusion Models (Blue)**. The visualization demonstrates that while high accuracy is achieved overall (strong diagonal), misclassifications are predominantly **intra-family** (e.g., between Glide variants), whereas **inter-family** separation remains robust.